Target Detection from Dual Disparate Sonar Platforms Using Canonical Correlations

Mahmood R. Azimi-Sadjadi[a], J. Derek Tucker[a]

[a]Department of Electrical and Computer Engineering, Colorado State University,
1373 Campus Delivery Fort Collins, CO, USA 80524;

ABSTRACT

In this paper a new coherence-based feature extraction method for sonar imagery generated from two disparate sonar systems is developed. Canonical correlation analysis (CCA) is employed to identify coherent information from co-registered regions of interest (ROI's) that contain target activities, while at the same time extract useful coherent features from both images. The extracted features can be used for simultaneous detection and classification of target and non-target objects in the sonar images. In this study, a side-scan sonar that provides high resolution images with good target definition and a broadband sonar that generates low resolution images, but with reduced background clutter. The optimum Neyman-Pearson detector will be presented and then extended to the dual sensor platform scenarios. Test results of the proposed methods on a dual sonar imagery data set provided by the Naval Surface Warfare Center (NSWC) Panama City, FL will be presented. This database contains co-registered pair of images over the same target field with varying degree of detection difficulty and bottom clutter. The effectiveness of CCA as the optimum detection tool is demonstrated in terms of probability of detection and false alarm rate.

Keywords: Canonical correlation analysis, disparate sensor platform, sonar imagery, target detection

1. INTRODUCTION

A critical need of the U.S. Navy is the development of a reliable, efficient and robust underwater target detection and classification system that can operate with multiple disparate sensor systems. In a surveillance area there could be multiple UUV's each equipped with a wide variety of sensors including different types of sonar, magnetics, or electro-optical systems or a single UUV equipped with multiple sensors. Preliminary detection, feature extraction, and object classification can be performed based upon the data collected using every sensory system on one or multiple vehicles. A final decision-making usually takes place at the central station using some type of a decision-level or a feature-level fusion. However, decision-making based upon individual sensory data typically leads to incomplete, degraded or biased decisions hence resulting in an unacceptable final detection and classification performance at the fusion center.

To allow collaborative decision-making among several disparate sonar (or other sensor) platforms, it is essential to detect and further scrutinize the information-bearing parts of the data collected by various sensory systems. This involves detecting, isolating and representing, in terms of some pertinent attributes, the *coherent* information among the multiple data sets. This is an extremely challenging problem due to disparate nature of the problem. To develop such a system-level solution, new methodologies are needed to: (a) collaboratively detect and agree on threats occurring within the field of view of the sensors, (b) perform collaborative feature extraction to capture common target attributes from multiple sensor platforms, (c) perform object classification and identification, (d) and finally develop a single integrated target assessment picture based upon the detected, localized and classified targets from multiple disparate sensors.

The existing work in the area of target detection from sonar imagery has primarily been focused on one sonar platform, with fusion across multiple algorithms. The method in[1,2] utilizes a nonlinear matched filter to identify mine-size regions in the sonar image that match the target signature. For each detected region, several features

Further author information: (Send correspondence to Dr. M. R. Azimi-Sadjadi)
M. R. Azimi: E-mail: azimi@engr.colostate.edu, Telephone: 1 970 491 7956
J. D. Tucker: E-mail: dtucker@engr.colostate.edu, Telephone: 1 970 491 1518

are extracted based on the size, shape, and strength of the target signature. A stepwise feature selection process is then used to determine the subset of features that maximizes the probability of detection and classification. A k-nearest neighbor and an optimal discrimination filter classifier are used to classify each feature vector and the decisions of the two classifiers are fused for the final decision. In,[3] a method was proposed that segments the sonar images into "sub-frames" of which each frame is adaptively thresholded to identify the target structure. Geometric features are then extracted from contiguous target structure ROI's within the sub-frame. Classification of each region as target or non target is done through a multi-level weighted scoring-based classification system. An adaptive clutter filter detector was presented in[4] which exploits the difference in correlation characteristics between clutter and targets. After detection, features are extracted and orthogonalized. Classification is then performed on the orthogonalized feature set using an optimal Bayesian classifier. Chandran in[5] presented the use of a matched filter designed to capture the target structure. Higher order spectra are extracted from the phase of the Fourier transform as the feature set to classify objects using a k-nearest neighbor classifier, a minimum distance classifier, and a threshold classifier based on the minimum and maximum values of a feature obtained over all classes, and the final decisions are fused.

More recently CCA has been applied to high resolution side-scan sonar imagery.[6] CCA allows one to quantify the changes between a background image versus when a target is present in the background and at the same time extract useful features for target classification without the need to perform separate detection and feature extraction. The previous work applied CCA to only one sonar image where both data channels were formed from an ROI in the image. The CCA-based detector was able to generate an average detection rate of 97% with a 3% false alarm rate with an average of 116 detections per image, 201 detections per image, and 213 detections per image on data sets with low, medium, and high density of background clutter and bottom complexity, respectively.

The work presented in this paper extends the CCA-based coherent framework in[6] for use with two images from two sensors operating at two different frequencies and spatial resolutions. For dual sonar platforms, the CCA data channels consist of ROI's of co-registered sonar images. In this case, canonical coordinate decomposition[7,8,6] provides an ideal framework for simultaneous coherent detection and feature extraction of target attributes that present in both images. These extracted canonical correlations for each pair of ROI's provide a coherence (or incoherence) measure that can be used to determine if a target is present (or absent) in the processed ROI's. Our *detection hypothesis* in this multi-sensor coherence analysis is that presence of objects in the multi-platform sonar data leads to high level of mutual information or coherence measure comparing to that of the background clutter only. The data set used in this study was provided by the NSWC-Panama City and consists of high-resolution side-looking sonar imagery that contains either no targets, one target, or multiple targets along with a broadband side-looking sonar imagery co-registered over the same region.

This paper is organized as follows: Section 2 reviews the optimum Neyman-Pearson detector for Gaussian random vectors and the CCA version of the detector. Section 3 describes the current problem with dual disparate sensors and extends the detector presented in Section 2. In Section 4, the results of using CCA to detect underwater targets from dual disparate sonar images will be presented. Finally, conclusions and observations are made in Section 5.

2. A REVIEW OF CCA-BASED DETECTOR

A classical detection problem,[9] is to decide between two hypothesis, namely the one of noise only and the other of signal plus noise. Assume we have an observation $\mathbf{y} \in \mathbb{R}^m$ which is a normal random vector with zero mean and covariance matrix R. We wish to test the hypothesis $H_0 : R = R_0$ i.e. noise alone versus $H_1 : R = R_1$ i.e signal plus noise, $R_1 = R_0 + R_s$ where R_0 is the covariance matrix of the noise alone and R_s is the covariance matrix of the signal. In other words, we want to decide between $H_0 : \mathbf{y} = \mathbf{n}$ and the alternative $H_1 : \mathbf{y} = \mathbf{s} + \mathbf{n}$.

The log-likelihood ratio that minimizes the risk involved in deciding between H_0 and H_1[9] is

$$\begin{aligned} \gamma(\mathbf{y}) &= \begin{cases} 1 \sim H_1, & l(\mathbf{y}) > l_0 \\ 0 \sim H_0, & l(\mathbf{y}) \leq l_0 \end{cases} \\ l(\mathbf{y}) &= \mathbf{y}^H Q \mathbf{y} \text{ with } Q = R_0^{-1} - R_1^{-1}, \end{aligned} \tag{1}$$

matrix Q can alternatively be expressed as

$$Q = R_0^{-H/2}(I - S^{-1})R_0^{-1/2}, \tag{2}$$

where S is defined as

$$S = R_0^{-1/2}R_1R_0^{-H/2}. \tag{3}$$

Now, we can rewrite $l(\mathbf{y})$ as,

$$l(\boldsymbol{\nu}) = \boldsymbol{\nu}^H(I - S^{-1})\boldsymbol{\nu}, \tag{4}$$

where $\boldsymbol{\nu} = R_0^{-1/2}\mathbf{y}$. The transformed vector $\boldsymbol{\nu}$ is also normal with zero mean and covariance matrix $R = I$ under H_0, and $R = S$ under H_1 i.e. $E_{H_0}[\boldsymbol{\nu}\boldsymbol{\nu}^H] = I$ and $E_{H_1}[\boldsymbol{\nu}\boldsymbol{\nu}^H] = S$, where E_{H_0} and E_{H_1} represent the expectation operation under H_0 and H_1, respectively.

The J-divergence[9] between the two hypothesis, which can be used as a measure of detectability, is

$$\begin{aligned} J &= E_{H_1}[l(\boldsymbol{\nu})] - E_{H_0}[l(\boldsymbol{\nu})] && (5)\\ &= tr(I - S^{-1})E_{H_1}[\boldsymbol{\nu}\boldsymbol{\nu}^H] - tr(I - S^{-1})E_{H_0}[\boldsymbol{\nu}\boldsymbol{\nu}^H] \\ &= tr(I - S^{-1})S - tr(I - S^{-1})I \\ &= tr(S + S^{-1} - 2I), && (6)\end{aligned}$$

where $tr(\cdot)$ denotes the trace operation on a matrix. Thus, the J-divergence depends only on the diagonal elements of S and S^{-1}. However, matrix S can be decomposed using singular value decomposition (SVD) as

$$S = R_0^{-1/2}R_1R_0^{-H/2} = U\Lambda U^H, \tag{7}$$

where Λ is a diagonal matrix with diagonal elements λ_i, that are the eigenvalues of S, and U is an eigenvector matrix containing the corresponding eigenvectors in its column space. This implies that $(R_0^{-H/2}U, \Lambda)$ solves the following generalized eigenvalue problem

$$R_1R_0^{-H/2}U = R_0R_0^{-H/2}U\Lambda. \tag{8}$$

Now, using the cyclic property of the trace and (7) the J-divergence in (6) can be rewritten as

$$\begin{aligned} J &= tr(\Lambda + \Lambda^{-1} - 2I) \\ &= \sum_{i=1}^{m}(\lambda_i + \lambda_i^{-1} - 2). && (9)\end{aligned}$$

Thus, solving the eigenvalue problem in (8) enables us to compute not only the J-divergence in (9) for detectability test but also the likelihood function in (4) for detection.

This detection problem can be cast in the CCA framework[10] in which the log-likelihood is expressed in terms of the canonical coordinates and the extracted canonical correlations and the J-divergence is expressed in terms of the canonical correlations. Figure 1 shows how the two-channel CCA can be used as an optimal detector. Under H_1 the composite covariance matrix for $\mathbf{z}^H = [\mathbf{x}^H\mathbf{y}^H]$ may be written as

$$R_{zz} = E[\mathbf{z}\mathbf{z}^H] = \begin{bmatrix} R_{xx} = R_0 & R_{xy} = R_0 \\ R_{yx} = R_0^H & R_{yy} = R_s + R_0 \end{bmatrix} \tag{10}$$

Then, the composite covariance matrix, R_{zz} may be taken to block-tridiagonal form as follows:[7]

$$\begin{bmatrix} F^H & 0 \\ 0 & G^H \end{bmatrix} \begin{bmatrix} R_{xx}^{-1/2} & 0 \\ 0 & R_{yy}^{-1/2} \end{bmatrix} R_{zz} \begin{bmatrix} R_{xx}^{-H/2} & 0 \\ 0 & R_{yy}^{-H/2} \end{bmatrix} \begin{bmatrix} F & 0 \\ 0 & G \end{bmatrix} = \begin{bmatrix} I & K \\ K & I \end{bmatrix} \tag{11}$$

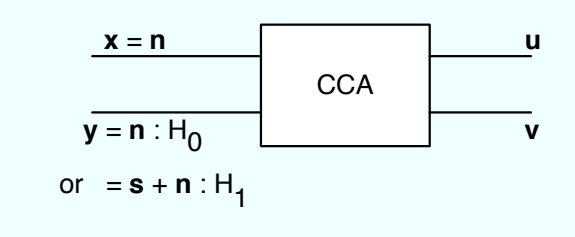

Figure 1. CCA used as an optimal detector.

Using the SVD of the coherence matrix $C = R_{xx}^{-1/2} R_{xy} R_{yy}^{-H/2} = R_{xx}^{H/2}(R_{xx} + R_{nn})^{-H/2} = R_0^{H/2} R_1^{-H/2}$

$$FKG^H = C \tag{12}$$

where F and G are orthogonal matrices, i.e. $F^H F = FF^H = I$ and $G^H G = GG^H = I$, and $K = diag[k_1, \cdots, k_l]$ is the canonical correlation matrix of *canonical correlations* k_i's.

The transformation

$$\begin{bmatrix} \mathbf{u} \\ \mathbf{v} \end{bmatrix} = \begin{bmatrix} F^H & 0 \\ 0 & G^H \end{bmatrix} \begin{bmatrix} R_{xx}^{-1/2} & 0 \\ 0 & R_{yy}^{-1/2} \end{bmatrix} \begin{bmatrix} \mathbf{x} \\ \mathbf{y} \end{bmatrix} \tag{13}$$

resolves $\mathbf{z}^H = [\mathbf{x}^H \mathbf{y}^H]$ into their canonical coordinates $\mathbf{w}^H = [\mathbf{u}^H \mathbf{v}^H]$, with composite covariance matrix

$$R_{ww} = E[\mathbf{w}\mathbf{w}^H] = \begin{bmatrix} R_{uu} = I & R_{uv} = K \\ R_{vu} = K & R_{vv} = I. \end{bmatrix} \tag{14}$$

Now, using (4) and expressing $(I - S^{-1})$ in terms of the squared coherence matrix $CC^H = R_0^{H/2} R_1^{-1} R_0^{1/2}$ yields[10]

$$l(\mathbf{y}) = (R_{xx}^{-1/2}\mathbf{y})^H([(CC^H)^{-1} - I]^{-1} - CC^H)(R_{xx}^{-1/2}\mathbf{y}) \tag{15}$$

which can further be expressed[10] in term of canonical correlation matrix K as

$$l(\mathbf{y}) = (G^H R_{yy}^{-1/2}\mathbf{y})^H([I - K^2]^{-1} - I)(G^H R_{yy}^{-1/2}\mathbf{y}) \tag{16}$$

or

$$l(\mathbf{v}) = \mathbf{v}^H([I - K^2]^{-1} - I)\mathbf{v} \tag{17}$$

This log-likelihood ratio is now expressed in the canonical coordinates $\mathbf{v} = G^H R_{yy}^{-1/2}\mathbf{y}$ and $l(\mathbf{v})$ is the weighted sum of the magnitude-squared of the canonical coordinates weighted by canonical correlation-dependent weights. That is,

$$l(\mathbf{v}) = \sum_{i=1}^{m} |v_i|^2 \left(\frac{k_i^2}{1 - k_i^2}\right) \tag{18}$$

where $v_i = g_i^H R_{yy}^{-1/2}\mathbf{y}$ and g_i is the i^{th} column of the matrix G.

It can be shown[10] that the J-divergence between H_1 and H_0 can be expressed in terms of the K matrix or canonical correlations i.e.,

$$J = tr([I - K^2]^{-1} - I - K^2) = \sum_{i=1}^{m} \frac{k_i^4}{1 - k_i^2}. \tag{19}$$

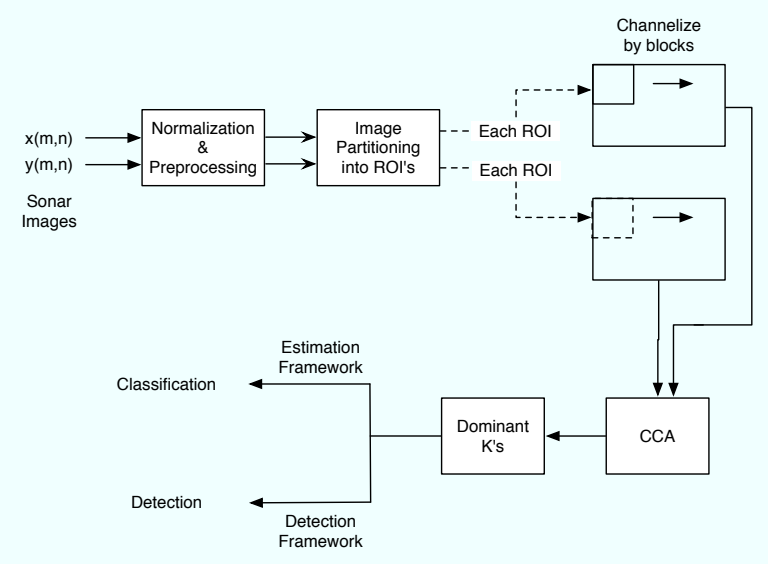

Figure 2. Coherent-Band detection and feature extraction from Dual Disparate Sonar Platform.

The function $\frac{k_i^4}{1-k_i^2}$ is non-increasing in the interval $(0, 1]$. *Consequently the rank-r detector that maximizes the divergence is the detector that uses the canonical coordinates corresponding to r dominant canonical correlations* $k_1, \cdots, k_r$. The divergence between the two hypothesis considering r dominant canonical correlations is,

$$J_r = \sum_{i=1}^{r} \frac{k_i^4}{1-k_i^2}. \tag{20}$$

Thus, for building low-rank detectors, only the dominant canonical coordinates need to be retained in order to find the coherence between the two data channels $\mathbf{x}$ and $\mathbf{y}$.

3. CCA COHERENT ANALYSIS FOR DUAL-PLATFORM SONAR IMAGERY

In this section, the coherent detection and feature extraction using the two-channel CCA[7] is applied to pairs of co-registered sonar images. The proposed method allows for simultaneous target detection and feature extraction even when target signatures are very subtle. The pair of sonar images, which cover the same area with possibly different spatial resolution and contrast, form the two-channels in the CCA processing. Owing to the fact that different sonar platforms observe the same area at different elevation, grazing angle, beamwidth, and frequency characteristics the target returns are more coherent than those of the background (*detection hypothesis*). CCA can isolate and represent these coherent (or common) features between the two data channels. Once the common features between the two sonar images are identified, the *coherence pattern* represented by the dominant canonical correlations can be used for subsequent classification (*classification hypothesis*) as the coherent information is captured in only few dominant canonical correlations corresponding to the dominant canonical coordinates.[10] It is interesting to note that using these coherent features one can easily generate a pair of images that illustrate the components of one sonar image that are highly coherent with the second sonar image and vice versa.

The first system is a high-frequency side-scan sonar that produces high resolution imagery while the second system is a broadband sonar. In the high resolution imagery of the first sonar, targets typically have good definitions with prominent highlights and shadows though clutter is also prominent. In the broadband sonar images the target highlight still shows up while clutter is not as prominent. Thus, the idea behind using CCA is to exploit the high coherence between the two sonar images when targets are present. As mentioned before, using CCA the canonical correlation features that capture this coherence property remain unchanged to perspective transformation on the images, which could be caused by variations in grazing angle and object orientation with

respect to the sonar platforms. Moreover, the beamformed complex-valued data of the sonar systems are used. Clearly, the capability to process complex-valued data and retain valuable phase information is another benefit of the CCA framework.

To perform CCA, the two pre-processed and co-registered sonar images are first partitioned into overlapping regions of interest (ROI's) of different sizes determined by the sonar resolution (see Figure 2). The corresponding ROI's of the two images are, in turn, partitioned into blocks of size $m \times n$ and $m' \times n'$ ($m \neq m'$ and $n \neq n'$ if the sonar systems have different resolution). The blocks of the two images form different realizations of the two random vectors, $\mathbf{x}$ and $\mathbf{y}$, representing the two data channels in the CCA. The idea here is to look for common or coherent attributes in a pair of ROI's that can be used to relate one channel to the other. Specifically, for background ROI's high level of coherence does not typically exist. Clearly, when both $\mathbf{x}$ and $\mathbf{y}$ are over a target there will be a higher coherence (measured by the extracted canonical correlations) than over a non-target.

Note that the way CCA is applied to this dual sensor platform detection problem is different than that presented in Section 2. In this case the H_0 hypothesis relates to the case where the ROI's cover background only while H_1 corresponds to the case where both ROI's contain target (signal) and background. That is, $H_0 : \begin{bmatrix} \mathbf{x} \\ \mathbf{y} \end{bmatrix} = \begin{bmatrix} \mathbf{n}_1 \\ \mathbf{n}_2 \end{bmatrix}$ i.e. noise alone versus $H_1 : \begin{bmatrix} \mathbf{x} \\ \mathbf{y} \end{bmatrix} = \begin{bmatrix} \mathbf{s}+\mathbf{n}_1 \\ \mathbf{s}+\mathbf{n}_2 \end{bmatrix}$. It is assumed that $\mathbf{n}_1, \mathbf{n}_2$ and $\mathbf{s}$ are mutually uncorrelated. With these hypothesis the derivations of the log-likelihood and J-divergence in the previous section no longer hold. For these hypothesis, the new covariance matrices, $\bar{R}_0$ and $\bar{R}_1$ can be defined as

$$\bar{R}_0 = \begin{bmatrix} R_n & 0 \\ 0 & R_n \end{bmatrix} \text{ and } \bar{R}_1 \begin{bmatrix} R_s + R_n & R_s \\ R_s & R_s + R_n \end{bmatrix} \tag{21}$$

where $E[\mathbf{n}_1\mathbf{n}_1^H] = E[\mathbf{n}_2\mathbf{n}_2^H]$, $R_n = R_0$, and $E[\mathbf{s}\mathbf{s}^H] = R_s + R_n = R_1$ as defined in Section 2.

The log-likelihood ratio that minimizes the risk involved in deciding between H_0 and H_1 is

$$\begin{aligned} \gamma(\mathbf{z}) &= \begin{cases} 1 \sim H_1, & l(\mathbf{z}) > \bar{l}_0 \\ 0 \sim H_0, & l(\mathbf{z}) \leq \bar{l}_0 \end{cases} \\ l(\mathbf{z}) &= \mathbf{z}^H \bar{Q} \mathbf{z} \text{ with } \bar{Q} = \bar{R}_0^{-1} - \bar{R}_1^{-1}. \end{aligned} \tag{22}$$

where $\mathbf{z} = \begin{bmatrix} \mathbf{x} \\ \mathbf{y} \end{bmatrix}$.

The expectation of the likelihood $E[l(\mathbf{z})] = E[tr(\bar{Q}\mathbf{z}\mathbf{z}^T)] = tr(\bar{Q}E[\mathbf{z}\mathbf{z}^T])$ leads to the J-divergence,

$$\begin{aligned} J &= E_{H_1}[l(\mathbf{z})] - E_{H_0}[l(\mathbf{z})] && (23) \\ &= tr(\bar{Q}\bar{R}_1) - tr(\bar{Q}\bar{R}_0) \\ &= tr(-2I + \bar{R}_0^{-1}\bar{R}_1 + \bar{R}_1^{-1}\bar{R}_0), && (24) \end{aligned}$$

Using (21), we can relate the J-divergence in (24) to R_0 and R_1 defined in Section 2 or to matrix S. Let us first express $tr(\bar{R}_0^{-1}\bar{R}_1)$ in (24) as,

$$tr(\bar{R}_0^{-1}\bar{R}_1) = 2tr(R_0^{-1}R_1) = 2tr(S) = 2tr(\Lambda) \tag{25}$$

where S was defined in (3) with eigenvalue decomposition (7). Next we express $tr(\bar{R}_1^{-1}\bar{R}_0)$ and rewrite it as,

$$tr(\bar{R}_1^{-1}\bar{R}_0) = \begin{bmatrix} R_1 & R_s \\ R_s & R_1 \end{bmatrix}^{-1} \begin{bmatrix} R_0 & 0 \\ 0 & R_0 \end{bmatrix} \tag{26}$$

Before we take the inverse of $\bar{R}_1$, we decompose it as,

$$\begin{aligned}\begin{bmatrix} R_1 & R_s \\ R_s & R_1 \end{bmatrix} &= \begin{bmatrix} R_1 & R_1 \\ R_1 & R_1 \end{bmatrix} - \begin{bmatrix} 0 & R_0 \\ R_0 & 0 \end{bmatrix} \\ &= -\left(\begin{bmatrix} 0 & R_0 \\ R_0 & 0 \end{bmatrix} - \begin{bmatrix} I \\ I \end{bmatrix} R_1 \begin{bmatrix} I & I \end{bmatrix} \right) \end{aligned} \tag{27}$$

Now, using the matrix inversion lemma[11] the inverse of $\bar{R}_1$ in (26) becomes

$$-\left(\begin{bmatrix} 0 & R_0^{-1} \\ R_0^{-1} & 0 \end{bmatrix} - \begin{bmatrix} 0 & R_0^{-1} \\ R_0^{-1} & 0 \end{bmatrix} \begin{bmatrix} I \\ I \end{bmatrix} \left(-R_1^{-1} + \begin{bmatrix} I & I \end{bmatrix} \begin{bmatrix} 0 & R_0^{-1} \\ R_0^{-1} & 0 \end{bmatrix} \begin{bmatrix} I \\ I \end{bmatrix} \right)^{-1} \begin{bmatrix} I & I \end{bmatrix} \begin{bmatrix} 0 & R_0^{-1} \\ R_0^{-1} & 0 \end{bmatrix} \right). \tag{28}$$

Using the fact that $\begin{bmatrix} 0 & R_0^{-1} \\ R_0^{-1} & 0 \end{bmatrix} \begin{bmatrix} R_0 & 0 \\ 0 & R_0 \end{bmatrix} = \begin{bmatrix} 0 & I \\ I & 0 \end{bmatrix}$, we can now rewrite (26) as

$$tr(\bar{R}_1^{-1}\bar{R}_0) = -tr\left(\begin{bmatrix} R_0^{-1}(R_1^{-1} - 2R_0^{-1})^{-1} & R_0^{-1}(R_1^{-1} - 2R_0^{-1})^{-1} + I \\ R_0^{-1}(R_1^{-1} - 2R_0^{-1})^{-1} + I & R_0^{-1}(R_1^{-1} - 2R_0^{-1})^{-1} \end{bmatrix} \right). \tag{29}$$

Again, using the matrix inversion lemma we can write $(R_1^{-1} - 2R_0^{-1})^{-1} = R_1 - R_1(R_1 - \frac{1}{2}R_0)^{-1}R_1$. Thus, the diagonal blocks in (29) can be rewritten as $[R_0^{-1}R_1 - R_0^{-1}R_1(I - \frac{1}{2}R_1^{-1}R_0)^{-1}]$, leading to

$$tr(\bar{R}_1^{-1}\bar{R}_0) = -2tr(R_0^{-1}R_1 - R_0^{-1}R_1(I - \frac{1}{2}R_1^{-1}R_0)^{-1}) = -2tr(S - S(I - \frac{1}{2}S^{-1})^{-1}). \tag{30}$$

Using (25) and (30) the J-divergence in (24) becomes

$$J = tr(-2I + 2S(I - \frac{1}{2}S^{-1})^{-1}). \tag{31}$$

Using the fact that S has an eigenvalue decomposition with eigenvalue matrix Λ, (31) reduces to

$$J = tr(-2I + 2\Lambda(I - \frac{1}{2}\Lambda^{-1})^{-1}) = \sum_{i=1}^{n} -2 + \frac{4\lambda_i^2}{2\lambda_i - 1}. \tag{32}$$

Using the fact that the eigenvalues of S (λ_i) are related[10] to the squared canonical correlations (k_i^2) by $\lambda_i = \frac{1}{1-k_i^2}$ we can rewrite the new J-divergence in terms of the canonical correlations $k_i's$ as

$$J = \sum_{i=1}^{n} -2 + \frac{4}{1 - k_i^4}. \tag{33}$$

To express the log-likelihood in (22) in terms of R_0 and R_1 we can write $\bar{Q} = (\bar{R}_0^{-1} - \bar{R}_1^{-1})$ and plug in the result for $\bar{R}_1^{-1}$

$$\bar{Q} = \begin{bmatrix} R_0^{-1} + R_0^{-1}(R_1^{-1} - 2R_0^{-1})^{-1}R_0^{-1} & R_0^{-1} + R_0^{-1}(R_1^{-1} - 2R_0^{-1})^{-1}R_0^{-1} \\ R_0^{-1} + R_0^{-1}(R_1^{-1} - 2R_0^{-1})^{-1}R_0^{-1} & R_0^{-1} + R_0^{-1}(R_1^{-1} - 2R_0^{-1})^{-1}R_0^{-1} \end{bmatrix}. \tag{34}$$

Thus the log-likelihood becomes

$$l(\mathbf{z}) = \mathbf{z}^H \begin{bmatrix} R_0^{-1} + R_0^{-1}(R_1^{-1} - 2R_0^{-1})^{-1}R_0^{-1} & R_0^{-1} + R_0^{-1}(R_1^{-1} - 2R_0^{-1})^{-1}R_0^{-1} \\ R_0^{-1} + R_0^{-1}(R_1^{-1} - 2R_0^{-1})^{-1}R_0^{-1} & R_0^{-1} + R_0^{-1}(R_1^{-1} - 2R_0^{-1})^{-1}R_0^{-1} \end{bmatrix} \mathbf{z}. \tag{35}$$

If we choose $\boldsymbol{\eta} = \begin{bmatrix} R_0^{-1/2} & 0 \\ 0 & R_0^{-1/2} \end{bmatrix} \mathbf{z}$, then

$$l(\boldsymbol{\eta}) = \boldsymbol{\eta}^H \begin{bmatrix} I + (S^{-1} - 2I)^{-1} & I + (S^{-1} - 2I)^{-1} \\ I + (S^{-1} - 2I)^{-1} & I + (S^{-1} - 2I)^{-1} \end{bmatrix} \boldsymbol{\eta}. \tag{36}$$

The log-likelihood is now rewritten in terms of S and R_0 from the original problem.

Now expressing $I + (S^{-1} - 2I)^{-1}$ in terms of the squared coherence matrix $CC^H = R_0^{H/2} R_1^{-1} R_0^{1/2}$ yields,

$$l(\boldsymbol{\eta}) = \boldsymbol{\eta}^H \begin{bmatrix} 1/2I - 1/4((CC^H)^{-1} - 1/2I)^{-1} & 1/2I - 1/4((CC^H)^{-1} - 1/2I)^{-1} \\ 1/2I - 1/4((CC^H)^{-1} - 1/2I)^{-1} & 1/2I - 1/4((CC^H)^{-1} - 1/2I)^{-1} \end{bmatrix} \boldsymbol{\eta}. \tag{37}$$

which can further be expressed in term of canonical correlation matrix K as

$$l(\boldsymbol{\eta}) = \boldsymbol{\eta}^H \begin{bmatrix} F & 0 \\ 0 & F \end{bmatrix} \begin{bmatrix} 1/2I - 1/4(K^{-2} - 1/2I)^{-1} & 1/2I - 1/4(K^{-2} - 1/2I)^{-1} \\ 1/2I - 1/4(K^{-2} - 1/2I)^{-1} & 1/2I - 1/4(K^{-2} - 1/2I)^{-1} \end{bmatrix} \begin{bmatrix} F^H & 0 \\ 0 & F^H \end{bmatrix} \boldsymbol{\eta}. \tag{38}$$

Using the SVD of the coherence matrix $C = R_0^{H/2} R_1^{-H/2} = FKG^H$, it is easy to show[10] that $F^H R_0^{-1/2} = K^{-1} G^H R_1^{-1/2}$ and the log-likelihood can be rewritten in terms of the canonical coordinates as

$$l(\mathbf{w}) = \mathbf{w}^H \begin{bmatrix} 1/2I - 1/4(K^{-2} - 1/2I)^{-1} & 1/2K^{-1} - 1/4(K^{-1} - 1/2K)^{-1} \\ 1/2K^{-1} - 1/4(K^{-1} - 1/2K)^{-1} & 1/2K^{-2} - 1/4(I - 1/2K^2)^{-1} \end{bmatrix} \mathbf{w}, \tag{39}$$

where $\mathbf{w} = \begin{bmatrix} \mathbf{u} \\ \mathbf{v} \end{bmatrix}$ is the composite canonical coordinate vector. So now the log-likelihood is only in terms of the canonical coordinates $\mathbf{u}$ and $\mathbf{v}$ and the canonical correlations k_i's.

4. TEST RESULTS ON MULTI-PLATFORM SONAR IMAGERY

The CCA-based detector was applied to a dual sonar data set consisting of high-resolution side-looking sonar images as well as broadband sonar images. More information on high-resolution side-looking and broadband sonars can be found in[12,13] and in[14,15],respectively. The database contains 59 images containing 67 targets with some of the images containing more than one target. For the present study, the optimum ROI sizes for the first and second sonar imagery were experimentally chosen to be 72×112 pixels and 24×224, respectively. The images are then partitioned into ROI's with a 50% overlap along both range and cross-range directions. Each ROI is then channelized by a rectangular blocking scheme with the dimension of the blocks for the first (high resolution) and second (broadband) sonar images being 6×4 and 2×8 pixels, respectively. Then, canonical correlations are computed for each pair ROI's. These canonical correlations can be used for both detection and classification as mentioned before.

To show the separability of the dominant canonical correlations for ROI's that contain targets over background and those that contain only background, a test was conducted on the entire set of 67 target ROI's and a same size randomly selected set of ROI's containing only background clutter. The plots of 16 canonical correlations of ROI's containing targets and those containing background only are shown in Figure 3. As can be seen, there is good separation between targets and background, especially for dominant canonical correlations. This can be attributed to the greater coherence between $\mathbf{x}$ and $\mathbf{y}$ channels across the target ROI's versus those over background clutter where there is more randomness.

Using the first 8 canonical correlations the J-divergence measure was formed using (33) for for the entire target set and random set of backgrounds and is presented in Figure 4. From this set of targets and limited number of backgrounds the optimal threshold value was chosen to be 16.9. This scalar value was then used as a scalar detection measure. That is, any ROI whose J-divergence falls above 16.9 is flagged as a target and visa-versa. The detector was executed on the entire data set and 61 of the 67 targets were detected with an average of 23 false detections per image. It was observed that for those targets that were missed the coherence was low due to the fact that the target only appeared in one of the images. Overall, the detector performed extremely well given the small number of targets and non-targets used to form the detection threshold.

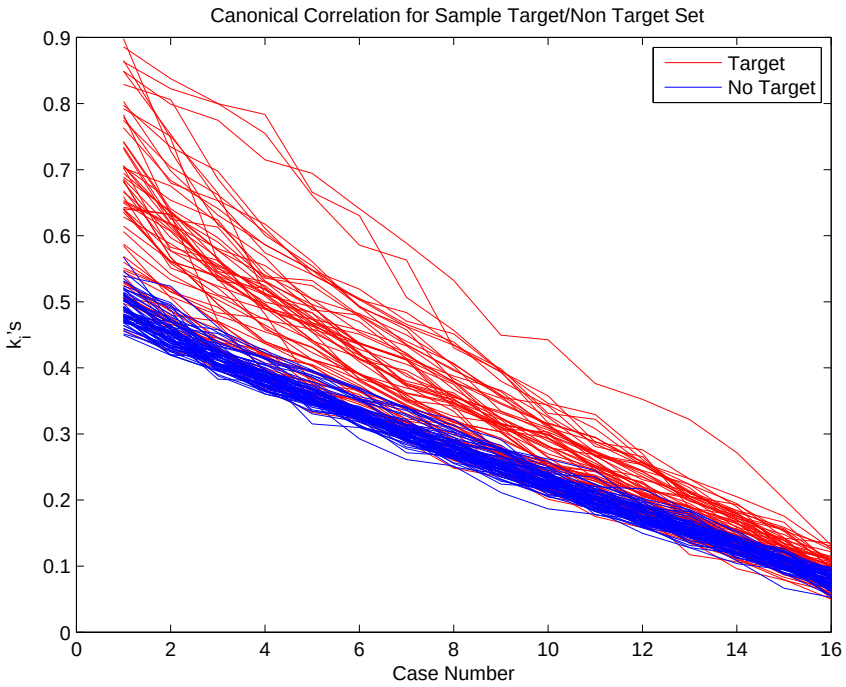

Figure 3. Plot of Canonical Correlations for Target and Background.

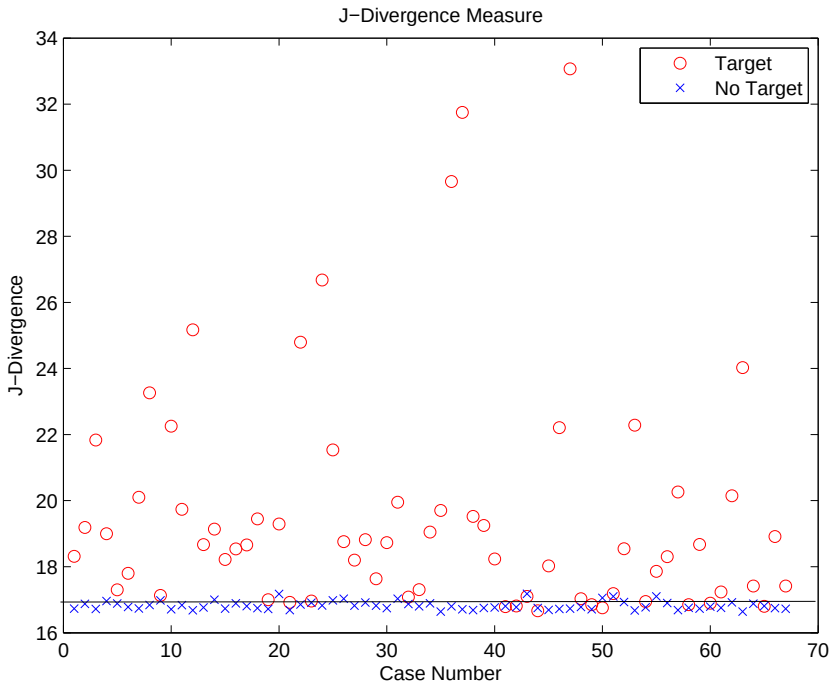

Figure 4. Separation of Target versus Background for J-divergence.

5. CONCLUSIONS AND OBSERVATIONS

In this paper, CCA was used as an optimum detector to detect underwater targets from dual-platform sonar imagery. In this framework, one of the CCA data channels is formed using the data from a high resolution side looking sonar while the other channel is formed using the data from a broadband sonar. It has been shown that when a target is present in the co-registered ROI's of the two sonar images there will be a large change in the coherence level compared to the case when there is no object. Further it has been shown that using the dominant canonical correlations, the J-divergence can be used as a scalar decision measure in order to separate the ROI's that contain a target from those that contain background only. Our experiments on the dual-platform sonar data set provided by the NSWC demonstrated that there is good separability among the dominant canonical correlations extracted over ROI's containing targets and those extracted from ROI's that do not contain targets. Overall, CCA did well in detecting 61 of the 67 targets in all of the images, while keeping the probability of detection high and false alarm rate low.

ACKNOWLEDGMENTS

This work was supported by the Office of Naval Research, Code 321OE under contract #N61331-06-C-0027

REFERENCES

[1] Dobeck, G. J., Hyland, J., and Smedley, L., "Automated detection/classification of sea mines in sonar imagery," *Proc. SPIE* **3079**, 90–110 (April 1997).

[2] Dobeck, G. J., "Fusing sonar images for mine detection and classification," *Proc. SPIE* **3710**, 602–614 (April 1999).

[3] Ciany, C. and Huang, J., "Data fusion of VSW CAD/CAC algorithms," *Proc. SPIE* **4038**, 413–420 (April 2000).

[4] Aridges, T., Libera, P., Fernandez, M., and Dobeck, G. J., "Adaptive filter/feature orthogonalization processing string for optimal LLRT mine classification in side-scan sonar imagery," *Proc. SPIE* **2765**, 110–121 (April 1996).

[5] Chandran, V., Elgar, S., and Nguyen, A., "Detection of mines in acoustic images using higher order spectral features," *IEEE Journal of Oceanic Engineering* **27**, 610–618 (July 2002).

[6] Tucker, J. D., Azimi-Sadjadi, M. R., and Dobeck, G. J., "Canonical coordinates for detection and classification of underwater objects from sonar imagery," *OCEANS 2007 - Europe* , 1–6, 18–21 (June 2007).

[7] Scharf, L. and Mullis, C., "Canonical coordinates and the geometry of inference, rate, and capacity," *IEEE Transactions on Signal Processing* **48**, 824–891 (March 2000).

[8] Pezeshki, A., Azimi-Sadjadi, M. R., and Scharf, L. L., "Undersea target classification using canonical correlation analysis," to appear in *IEEE Journal of Oceanic Engineering* .

[9] Scharf, L. L. and Van Veen, B. D., "Low rank detectors for Gaussian random vectors," *IEEE Trans. Acoust., Speech, Signal Process.* **35**, 1579–1582 (Nov 1987).

[10] Pezeshki, A., Scharf, L., Thomas, J. K., and Van Veen, B. D., "Canonical coordiantes are the right coordinates for low-rand gauss-gauss detection and estimation," *IEEE Trans. Signal Process.* **54**, 4817–4820 (Dec 2006).

[11] Golub, G. H. and Loan, C. F. V., [*Matrix Computations*], John Hopkins University Press, third ed. (1996).

[12] Rimski-Korsakov, N., Russak, Y., and Pavlov, R., "Simple digital system for side scan sonar data imaging," *Proc. Oceans'94* **1**, 643–645 (Sept 1994).

[13] Key, W., "Side scan sonar technology," *Proc. Oceans'00* **2**, 1029–1033 (Sept 2000).

[14] Butler, S., "Triply resonant broadband transducers," *Oceans '02 MTS/IEEE* **4**, 2334–2341 vol.4 (29-31 Oct. 2002).

[15] Butler, S., "High frequency triply resonant broadband transducer array development at nuwc," *OCEANS 2003. Proceedings* **5**, 2380 Vol.5– (22-26 Sept. 2003).